ornl

ORNL/TM-9949

OAK RIDGE NATIONAL LABORATORY

MARTIN MARIETTA

Ion Microprobe Mass Spectrometry Using Sputtering Atomization and Resonance Ionization: Annual Progress Report

D. E. Goeringer
W. H. Christie
H. S. McKown
D. L. Donohue

OPERATED BY
MARTIN MARIETTA ENERGY SYSTEMS, INC.
FOR THE UNITED STATES
DEPARTMENT OF ENERGY

Printed in the United States of America. Available from
National Technical Information Service
U.S. Department of Commerce
5285 Port Royal Road, Springfield, Virginia 22161
NTIS price codes—Printed Copy: A03; Microfiche A01

ORNL/TM-9949

Contract No. DE-AC05-84OR21400

Analytical Chemistry Division

ION MICROPROBE MASS SPECTROMETRY USING SPUTTERING ATOMIZATION AND RESONANCE IONIZATION: ANNUAL PROGRESS REPORT

D. E. Goeringer, W. H. Christie, H. S. McKown
and D. L. Donohue

Date Published - May 1986

Prepared by the
OAK RIDGE NATIONAL LABORATORY
Oak Ridge, Tennessee 37831
operated by
MARTIN MARIETTA ENERGY SYSTEMS, INC.
for the
U. S. Department of Energy

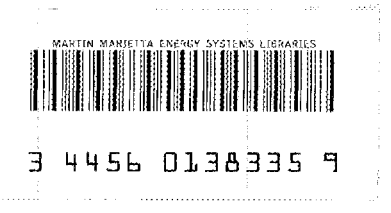

TABLE OF CONTENTS

List of Figures

ION MICROPROBE MASS SPECTROMETRY USING SPUTTERING ATOMIZATION AND RESONANCE IONIZATION

D. E. Goeringer, W. H. Christie, H. S. McKown
and D. L. Donohue*

Abstract

Resonance Ionization Mass Spectrometry (RIMS) utilizing ion beam sputtering atomization has been applied to the measurement of U and Sm. The goal is to produce an ultrasensitive analytical technique for measuring elements of environmental concern in small particles or inclusions. An ion microprobe mass analyzer (IMMA) has been modified to allow production of a sputtered atom plume through which high powered tunable laser radiation is directed. Ions of a given element are produced by a multistep resonance ionization process followed by extraction into a double-focusing mass spectrometer for detection. Data are presented showing mass and optical spectra obtained as well as the sensitivity of the technique.

*Present address: IAEA, Vienna, Austria

1. Introduction

Resonance Ionization Mass Spectrometry (RIMS) has recently been developed into a useful technique for isotopic ratio measurements. Studies performed in our laboratory[1-5] and elsewhere[6-13] have been reported for a variety of elements using thermal vaporization sources to produce the atom reservoir for laser-induced resonance ionization. Other methods of atomization have been reported, including a glow discharge,[14] laser ablation,[15] and ion beam sputtering.[16-18]

Ion beam sputtering is an attractive process for coupling with pulsed laser ionization because the process of atom formation can be highly controlled. Sputter rates for pure metals have been measured under differing conditions of incident ion beam composition, energy, angle, and current density. Knowledge of the energy and angular distribution of the sputtered atoms allows one to calculate the geometrical overlap between a sputter "plume" and a laser beam of given cross-section. In addition, when pulsed sputtering is utilized, the temporal overlap between the atomization and ionization can approach 100%. Provided the laser beam is sufficiently powerful to saturate the ionization process, the overall efficiency will allow 1 ion to be formed for every 50 or fewer atoms removed from the sample. Determination of isotope ratios then becomes a matter of extracting these ions into a suitable mass spectrometer, followed by pulse counting or pulse height detection.

The goal of ultrahigh sensitivity detection is important for monitoring trace elements in environmental samples such as U and Pu in airborne particulates. Particles may contain picogram to femtogram amounts of these elements. In order to obtain isotopic composition of the U or Pu, maximization of sampling and detection efficiencies is a necessary condition for this type of analysis.

To this end, a commercial ion microprobe mass analyzer (IMMA) has been interfaced with a tunable pulsed dye laser for carrying out resonance ionization mass spectrometry of sputtered atoms. The IMMA instrument has many advantages for this work, including a micro-focused primary ion beam (2 μm in diameter) of selected mass, complete sample manipulation and viewing capability, and a double-focusing mass spectrometer for separation and detection of the secondary or laser-generated ions. This paper will describe the changes necessary to adapt the IMMA instrument for resonance ionization, along with preliminary results for the elements Sm and U. Data are presented demonstrating the number and type of ions formed along with optical spectral information showing the wavelengths at which resonance ionization occurs.

2. Experimental

2.1. IMMA

The secondary ion mass spectrometer used in this work was manufactured by Applied Research Laboratories (Sunland, CA) and is based on the design of Liebl.[19] In essence, the instrument is two mass spectrometers. In the primary spectrometer a beam of ions generated via a Duoplasmatron ion source is accelerated, mass analyzed, and focused onto the surface of interest. Ions sputtered from the sample surface are directed into a double focusing mass spectrometer where mass analysis is accomplished. Modifications to the ion extraction lens system, which allow discrimination against sputtered secondary ions while allowing collection of laser-generated ions, are described in a following section. For this work the secondary mass analyzer was operated at mass resolutions ($M/\Delta M$) on the order of 200. Primary ions were generated by using a mixed gas consisting of approximately 2 atom % Ar, 34 atom % N_2 and 64 atom % O_2 in the duoplasmatron ion source. This allowed the sputter targets to be bombarded with operator-selected mass analyzed ion beams of Ar^+, N_2^+ or O_2^+.

To facilitate the ion optical changes, the indium metal seal, used to attach the microscope to the sputtering chamber, was replaced with a large viton o-ring. This provided a vacuum-worthy seal that allowed removal and replacement of the microscope in minutes when access to the sputtering chamber was desired.

2.2 Laser Source and Light Optics

The laser source used in this study was a Chromatix CMX-4 flashlamp-pumped dye laser with a bandwidth of approximately 3 cm^{-1} and an optical pulse width of about 1 μs. A useful wavelength range of approximately 580-610 nm was generated with the Rhodamine-6G dye used in all the experiments. The pulse energy measured directly at the laser

output was about 5 mJ with the available energy above the sample surface estimated to be from 10-50 times less. A stepping motor was attached to the micrometer-driven wavelength selection mechanism to permit reproducible spectral scans to be made under computer control. The wavelength calibration was performed by directing a portion of the laser beam into the bore of a Ne-filled U hollow cathode lamp and recording its optogalvanic spectrum. Least-squares regression analysis of the data for known Ne and U wavelengths produced a calibration slope of 5.39 $\pm$ 0.02 x 10^{-4} nm-step^{-1} and a standard deviation of the residuals of 0.04 nm.

The light optics used to position and focus the laser beam above the sample are diagrammed in Figure 1. The beam was spatially filtered and focused to approximately 0.05 cm diameter spot directly above the sample with a beam expander assembly housing a 10 μm pinhole. The horizontal and vertical positions of the beam relative to the sample surface were varied by an adjustable mirror mount. The elevation of the laser beam was lowered to a plane parallel and just above the sample surface by a periscope assembly mounted in the sample chamber.

2.3 Signal Processing

Photomultiplier anode pulses produced by individual ions reaching the Daly detector were processed by a preamplifier/discriminator. The resultant collection of pulses produced by a single laser shot was integrated into a single pulse approximately 10 μs wide by a variable gain and pulse-shaping amplifier as shown in Figure 2. The amplitude of this pulse is proportional to the number of ions produced by the laser shot. The output pulse was sampled by a gated integrator triggered by the sync pulse from the laser; the gate delay was adjusted to coincide with the output pulse which occurs approximately 30 μs after the laser sync pulse. The resultant DC output signal from the gated integrator was further processed by the data system.

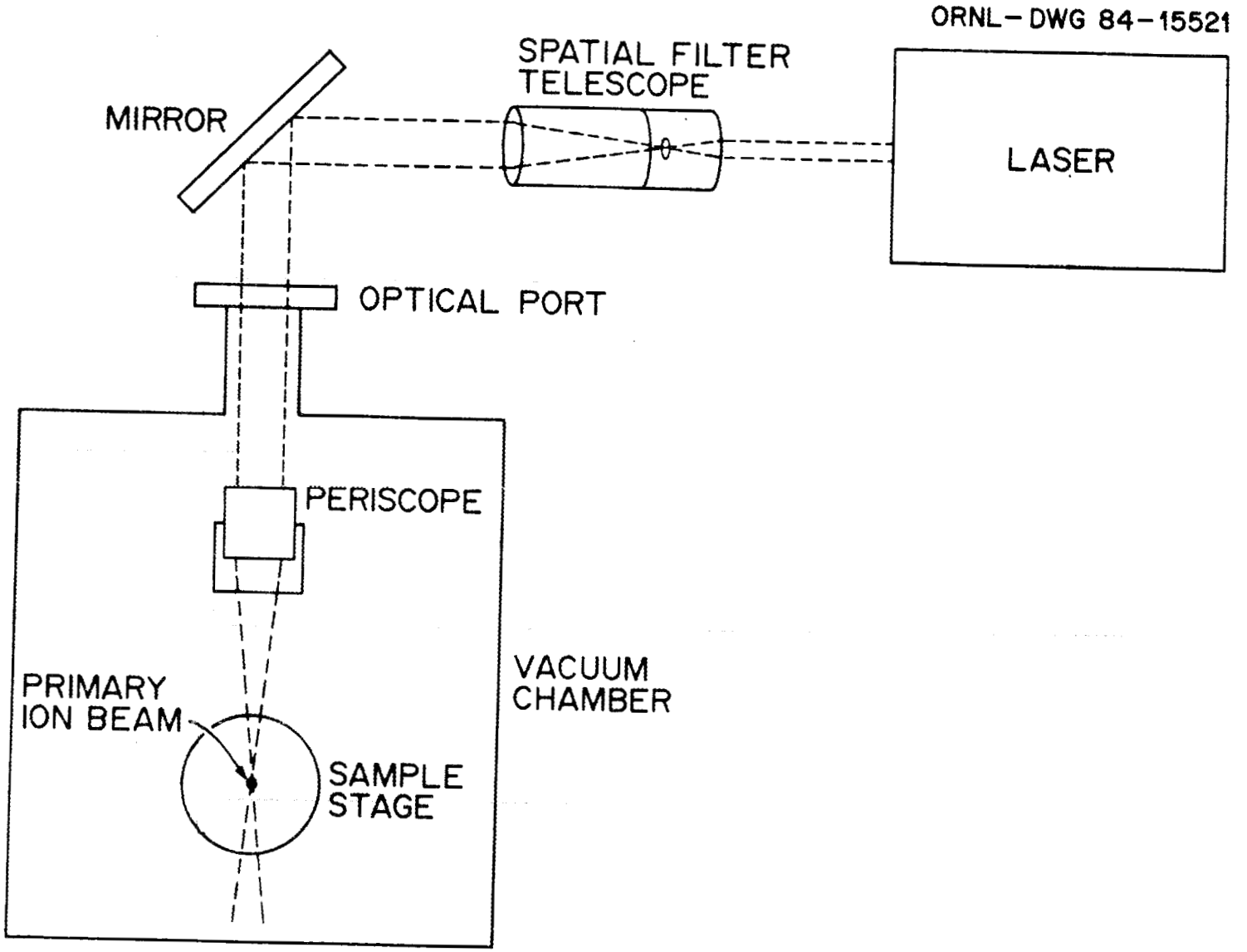

Fig. 1. Laser optics for resonance ionization of sputtered atoms

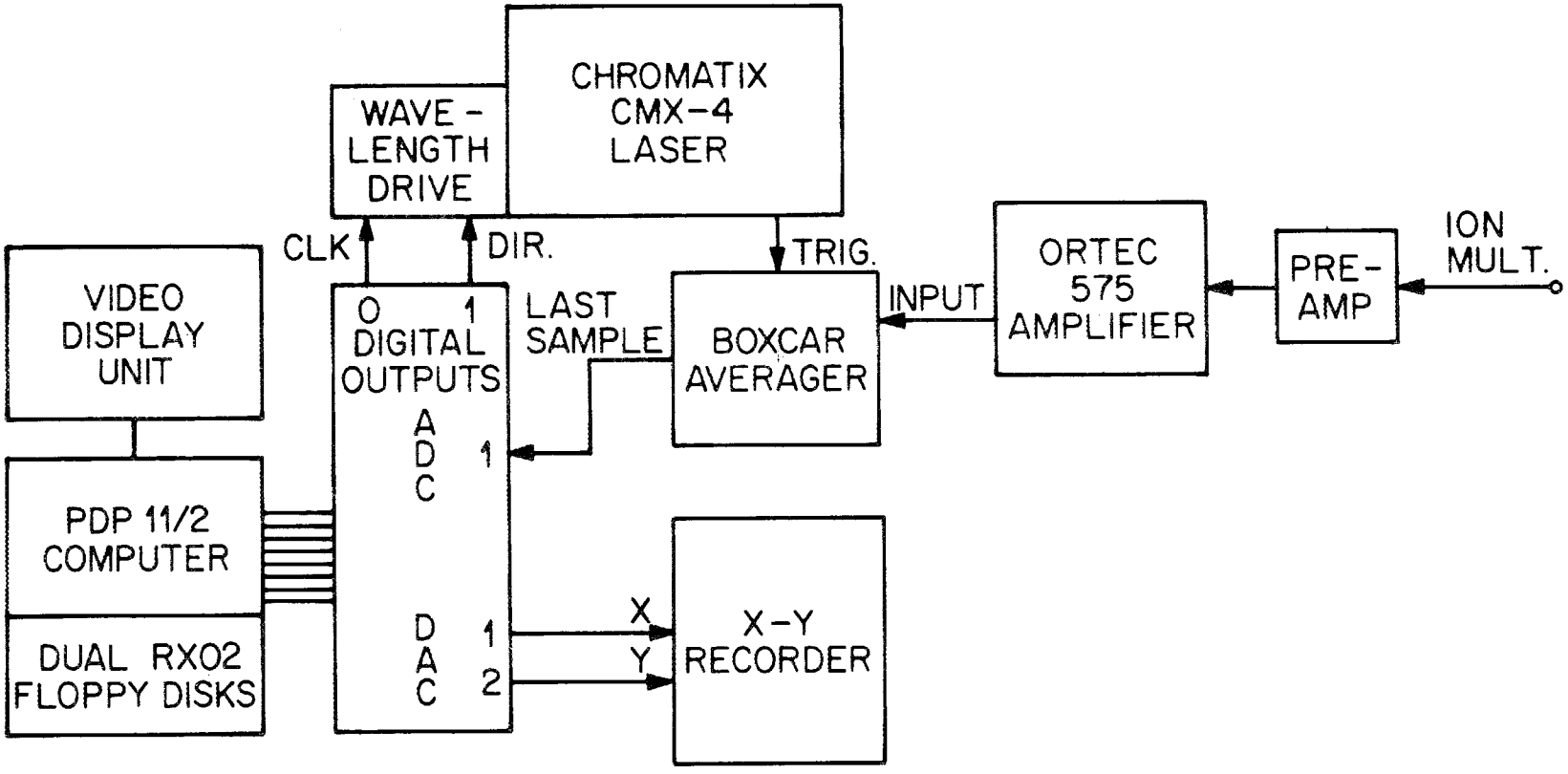

Fig. 2. Electronics for data acquisition and laser control

2.4 Data System

Data acquisition and control for the experiments were performed by an LSI-11/2 microcomputer housing an analog-to-digital converter (ADC), two digital-to-analog converters (DAC), and a 16-bit parallel I/O interface. The ADC samples the DC output of the gated integrator and converts it into a digital value. The parallel interface controls the direction and speed of the stepping motor attached to the wavelength micrometer drive of the laser. The DAC outputs drive an x-y scope for real-time display of spectra of an x-y plotter for post-acquisition recording of spectra.

2.5 Spectral Acquisition

Optical data were collected as the average of 15 laser shots per datum, with a 50-step ($\sim$0.027 nm) interval between data points. One thousand such data points, corresponding to a wavelength range of 27 nm, were collected for each optical spectrum.

Mass spectral data were obtained by scanning the secondary magnet via front panel controls while leaving the laser fixed at the resonant wavelength of the desired element. Data were acquired at 0.2 amu intervals with each datum representing the average of 15 laser shots.

2.6 Samples

Samples consisting of natural U and Sm metal embedded in low vapor pressure epoxy were polished until a smooth metallographic finish was obtained. The cross-sectional area of each metal sample was approximately 0.1 cm^2.

3. Results and Discussion

3.1 Ion Optics

The existing ion extraction optics of the IMMA instrument were designed to efficiently extract sputtered secondary ions produced at the sample surface as shown in Figure 3. The sample is held at a potential of +1500V relative to the extraction electrode which is at ground potential. The equipotential sufaces and ion trajectories were calculated by a computer routine SIMION[20] (details available from the authors). Curvature of the equipotential surfaces in the vicinity of the pickup electrode results in highly efficient steering of the sputtered secondary ions which exit at varying angles up to 45° from the normal and with energies ranging from 0 to 20 eV. Subsequent energy filtering by the electrostatic sector and mass dispersion in the magnetic sector result in a conventional secondary ion mass spectrum.

Figure 4 shows the result of forming the ions above the sample surface via resonance ionization while using the same extraction optics and conditions. These ions are affected differently by the field and are deflected too much. Most of them strike the inner surface of the extraction electrode and are lost. Even those which pass through the pickup electrode will have too much angular deviation from the ideal 45° angle to be refocused by subsequent ion lenses.

For this reason, new ion optics systems were studied using the SIMION program. One of the most successful designs is shown in Figure 5. The objective was to create a flat extraction field in the volume directly above the sample surface, with the field equipotential surfaces inclined at the desired 45° angle relative to the sample surface. To achieve this, a "pusher" electrode was added (shown to the right in the figure) and the pickup electrode itself was significantly changed. As can be seen, the equipotential surfaces are relatively flat

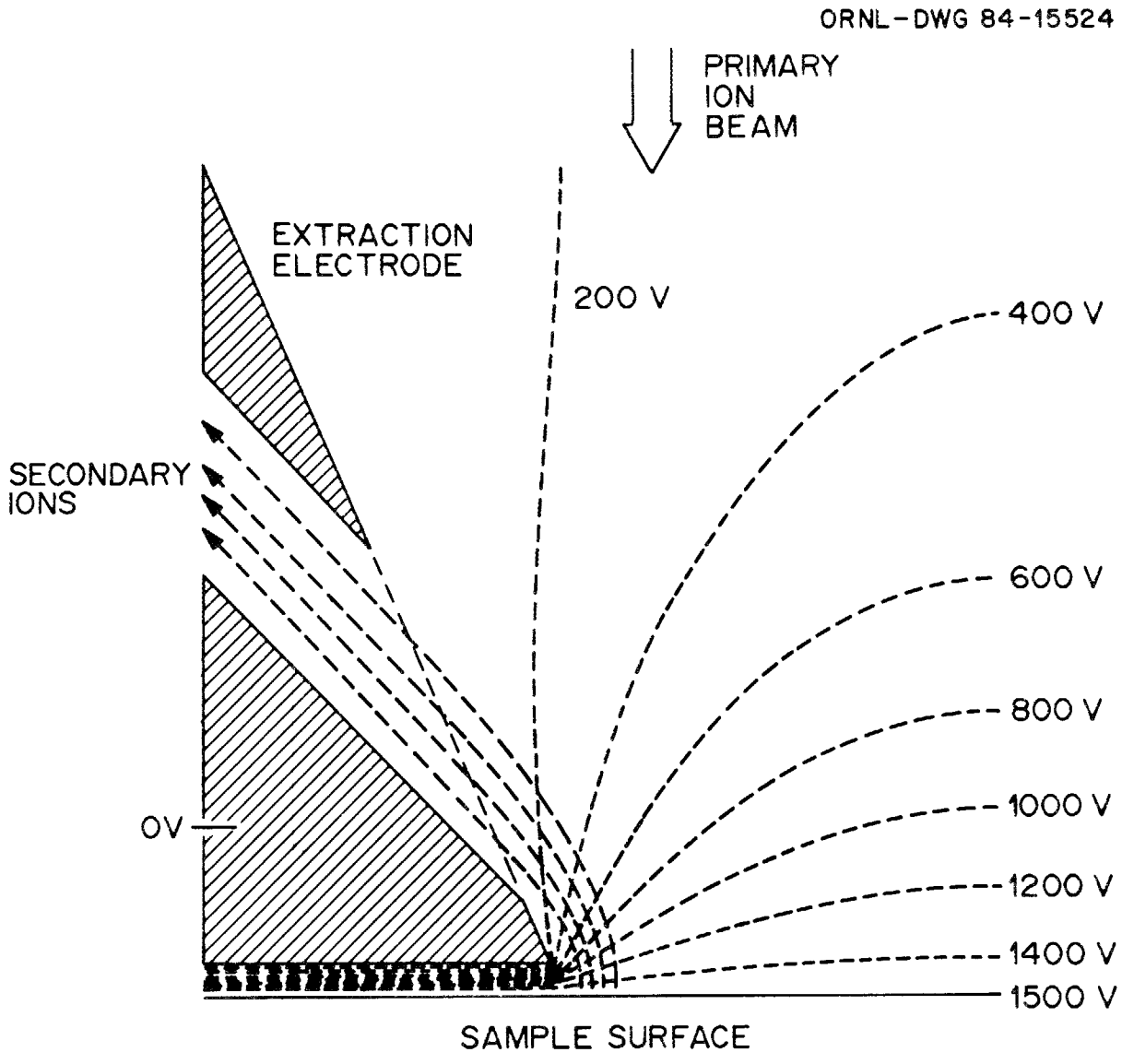

Fig. 3. Ion lens system for extraction of secondary ions produced by ion beam sputtering

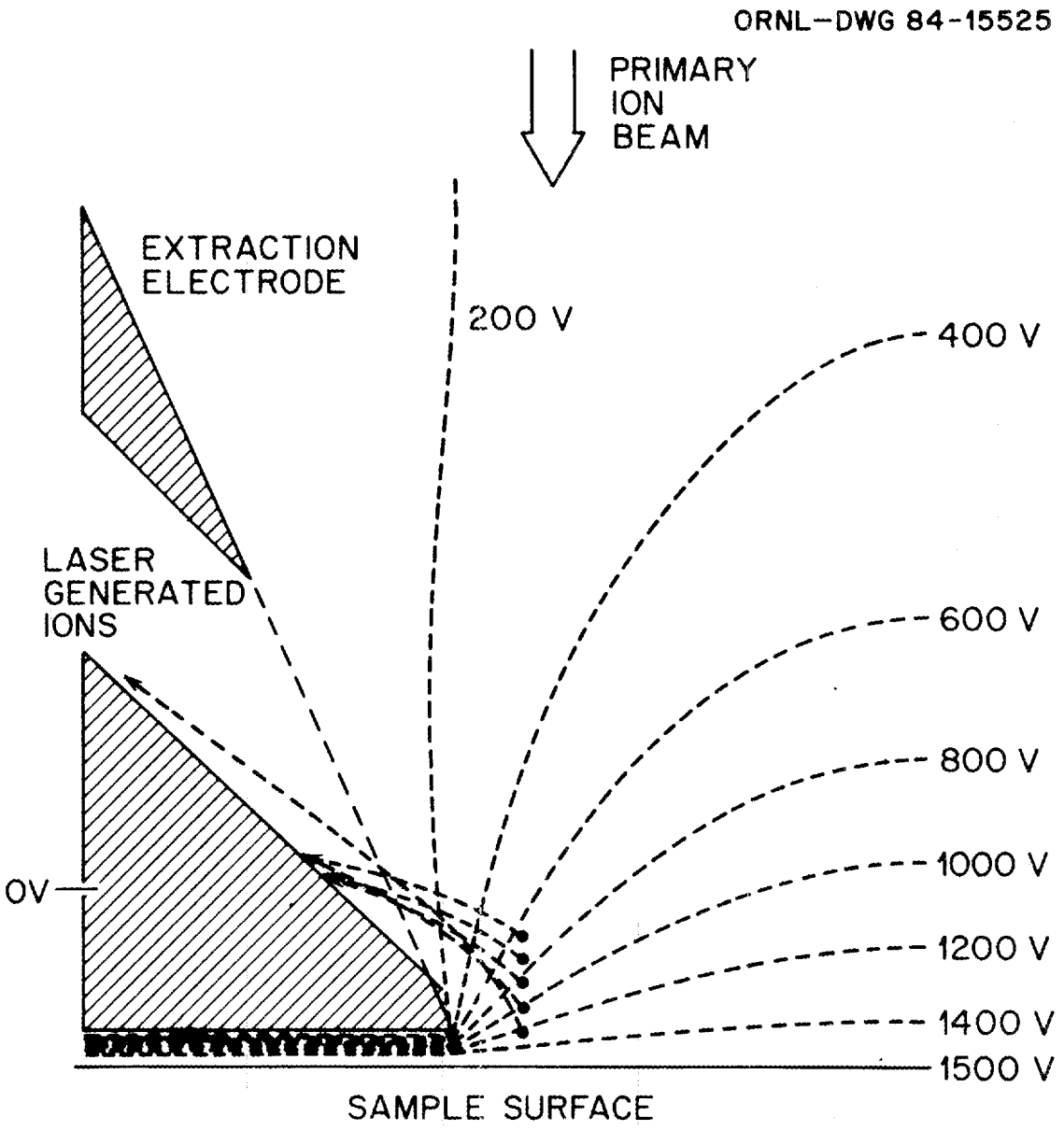

Fig. 4. Ion trajectories resulting from laser-generated ion formation above the sample surface

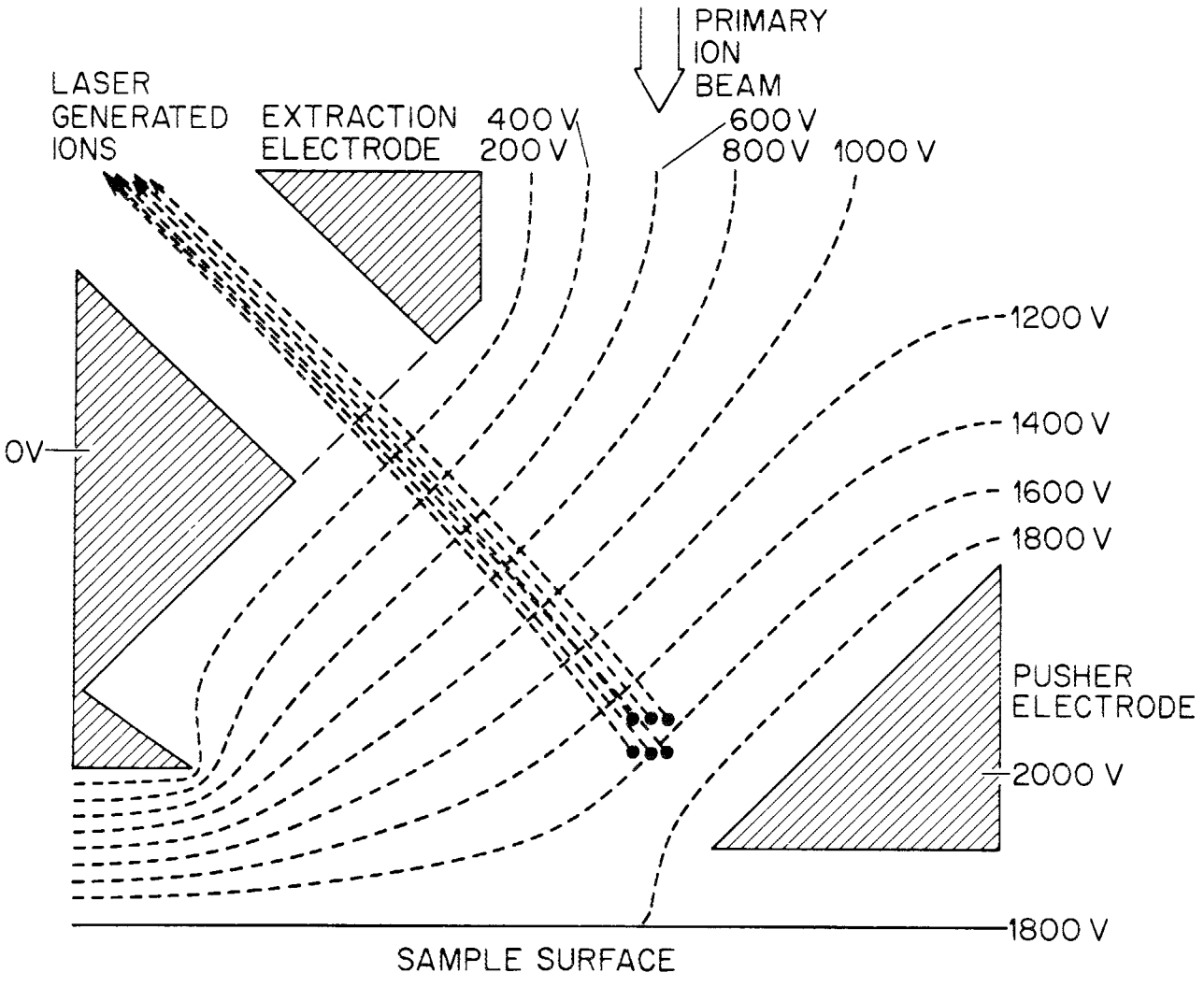

Fig. 5. Modified ion optics to extract and focus ions produced in a volume above the sample surface

in the region between the two electrodes, although they are less so directly above the sample surface. Ions formed in the volume element shown follow a nearly perfect trajectory through the pick-up electrode. This figure illustrates a possible problem in that ions formed in a finite volume will experience different extraction potentials and will have a spread of energies which would seriously affect the throughput or resolution of the secondary mass spectrometer. Other electrode designs are being tested which should reduce or eliminate this effect.

3.2 Sensitivity

The ARL ion microprobe is recognized as being a sensitive instrument when operated in low mass resolution mode ($M/\Delta M$) $\leq$ 200. Measurements from accurately doped ion implantation standards (e.g., B in Si) confirm this high sensitivity. For example, with a properly tuned instrument it is typical to detect approximately one B^+ ion for each 1000 sputtered B atoms from a B implanted silicon matrix. Our laboratory has two ARL microprobes and this provided convenient and useful intercomparison. The probe used in this work (RIMS) was a decommissioned instrument obtained from another laboratory and extensive work was required to get its sensitivity up to specification. The final design of the modified ion extraction lens system, which was optimized for laser-generated ions formed above the sputtering surface, gave a sensitivity for sputtered ions that was about 10% as efficient as the original ion optics optimized for sputtered ions.

An important feature of the ion microprobe instrument used in this study is the ability to use different sputtering species under closely similar conditions. Using an $O_2/N_2/Ar$ gas mixture in the duoplasmatron ion source allows the investigator to rapidly select sputtering beams of O_2^+, N_2^+, and Ar^+. Studies of the resonance ionization signals obtained using each of these bombarding species on U and Sm targets revealed that Ar^+ was a factor of 10-20 times more efficient

at producing sputtered atoms in the ground state than O_2^+ or N_2^+. This result is in qualitative agreement with that of Kimock, et al.[18] in which the population of ground state atoms in the sputter plume drops as oxygen exposure increases (for Ar^+ bombardment). More quantitative measurements of this effect will be the subject of future studies.

The ion bundle produced in a single laser pulse (nominally 1 μs long) was found to be 3 ± 1 μs wide at the detector following a delay of 23 μs (for Sm) or 30 μs (for U) due to time-of-flight through the secondary mass spectrometer. The number of ions in each bundle could be counted using a fast oscilloscope to monitor the output of the ion multiplier preamplifier. Individual ions produced a signal of approximately 1 V amplitude, with a 20 ns width. Bundles with less than 50 ions allowed reliable counting of the actual number of ions from the oscilloscope trace; those with more than 100 ions could not be counted with acceptable precision. An estimate of the number of ions in such large pulses could be obtained by measuring a number of individual pulses with the gated integrator/ADC system. From the relative standard deviation of these measurements, the number of ions per pulse could be deduced from the relationship:

$$RSD = \frac{\sqrt{n}}{n} \qquad (1)$$

where n is the total number of ions collected. The largest signals obtained for ^{238}U using Ar^+ bombardment were calculated to have > 100 ions per pulse while those for ^{152}Sm were found to have 40 ions per pulse. It is also important to note that the background signal from sputtered secondary ions was extremely low due to the time gating of the detection system and the region of ion formation discrimination of the modified ion extraction electrode.

An estimate of the sampling efficiency can be obtained from the conditions which gave > 100 U^+ ions per laser pulse. The current of Ar^+ ions incident on the surface was 21 na, or 1.3×10^{11} ions-sec^{-1}. However, due to the pulsed nature of the laser, only a small fraction of this current was effective in producing U atoms for the resonance ionization process. This fraction is determined by the average transit time of atoms through the laser volume (for short duration laser pulses) or by the actual length of the laser pulse (for pulse lengths of $\geq$ 100 ns). The above argument assumes a 0.1-0.01 cm laser beam diameter and an average kinetic energy of 10 eV for the U atoms. In the case reported here, the nominal laser pulse duration was 1 μs, which means that 1.3×10^5 Ar^+ ions incident on the surface resulted in > 100 U^+ ions being detected. Therefore, the gross efficiency of the sputtering-resonance ionization process was 1 ion detected for every 1300 Ar^+ ions striking the sample. To estimate the efficiency in terms of U^+ ions detected as a function of U atoms sputtered would require a knowledge of the sputter yield for U under the conditions of this study. Such measurements, though difficlt, are being pursued in order to define the degree of improvement necessary to reach the goal of 1 ion detected for every 50 atoms in the sample. The largest expected gain in efficiency should result from use of a larger, more powerful laser beam to saturate the resonance ionization process over a larger volume of the sputter plume.

3.3 Optical Spectra

Figure 6 shows the optical ionization spectra of Sm over the wavelength range 580-607 nm. The top spectrum was obtained using sputter atomization, while the lower spectrum resulted from heated thermal filament atomization (at 1500°C) taken under conditions similar to Ref. 2. The peaks observed for sputter atomization match quite closely with those from thermal atomization, with the exception of the line at 580.16 nm. This line is absent from the upper spectrum because

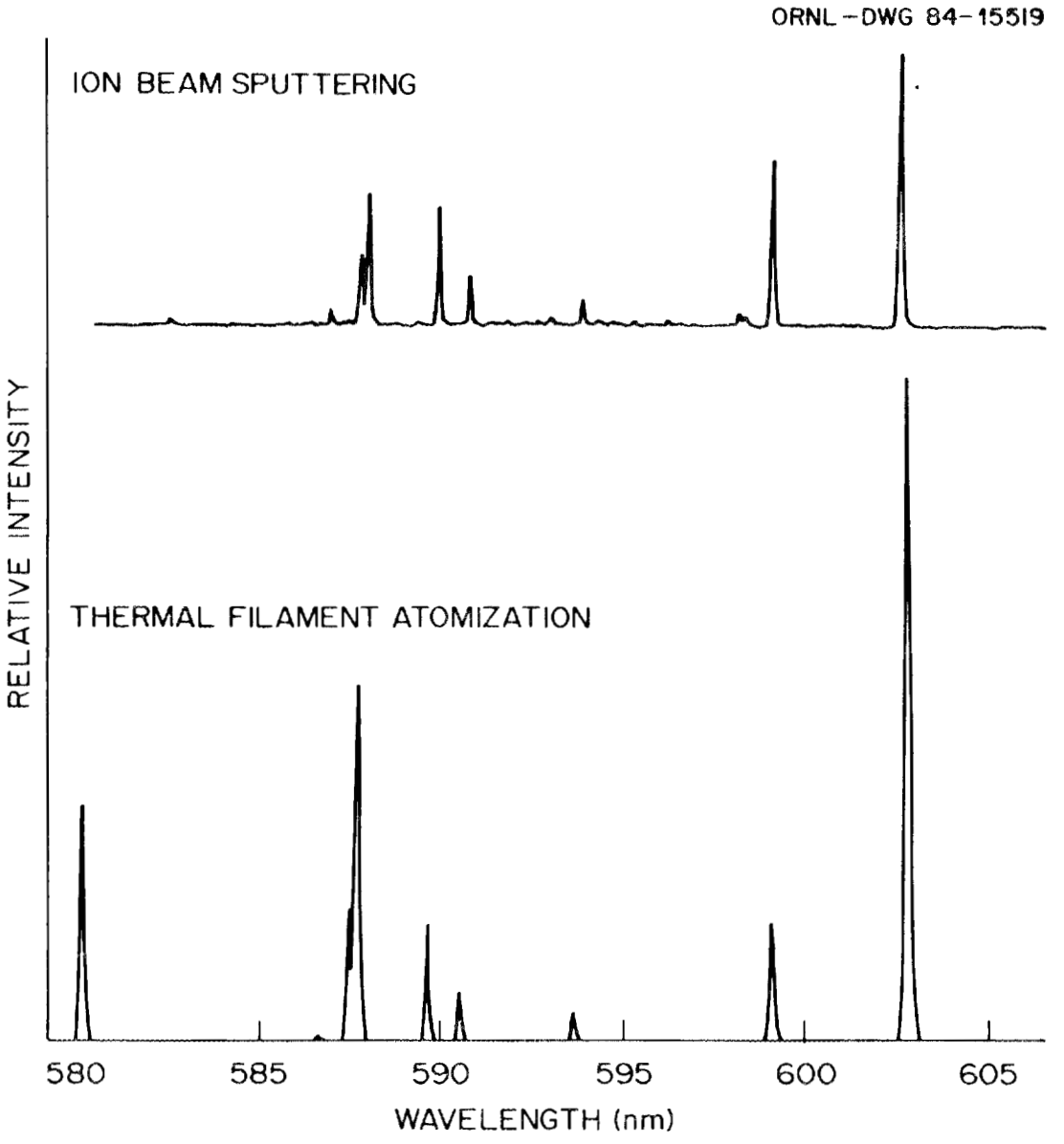

Fig. 6. Optical ionization spectra of ^{152}Sm atoms produced by ion beam sputtering (top) and thermal filament atomization (bottom)

of reduced bandwidth in the dye output spectrum due to lower power. The remainder of the spectral range was adequately covered as can be seen by the close match in relative intensity of the lines.

Table 1 shows the interpretation of the lines found with sputter atomization. In all cases, the lines originate in the ground state ^7F_n manifold of Sm, with a distribution of states resembling that of the thermal atomization process at 1500°C. The apparent ground state originating line at 599.11 nm is enhanced in the sputtering case relative to two lines originating from the $^7F_3$ level at 587.69 nm and 602.81 nm. This indicates a lower "temperature" of the atoms produced by sputtering, although in the absence of local thermal equilibrium, the ground state may be enhanced by decay of highly excited species a short time after the sputtering event, but before the ionizing laser is turned on.

The lines observed for Sm at these wavelengths can only result from a single-color three photon process. The ionization energy[21] of Sm is 45519 cm^{-1} compared to the energy range of the photons used (16500-17200 cm^{-1}). Provided that the interpretation in Table D2 is correct, the absorption of two photons would result in states which are 7000-12000 cm^{-1} below the ionization energy. A third photon absorption is therefore required before ionization would result. The sharp line nature of the peaks observed strongly suggests that resonant absorption occurs for the first two photons, proceeding through allowed upper energy levels about which nothing has been published. This also resembles the case for the actinide elements described in another report[22].

Figure 7 shows the spectra of U taken under conditions similar to those for Sm. The agreement between sputter atomization and thermal atomization is excellent. The interpretation of the lines in the thermal spectrum can be found elsewhere.[22] The two largest lines

Table 1. Interpretation of Sm Spectral Lines Using Sputter Atomization

Observed Spectral Features			Interpretation[21]		
Wavelength			Wavelength	$E_1 - E_2$	Term
(nm)	Intensity	(cm^{-1})	(nm)	(cm^{-1})	
586.67	W	17040.4	586.62	4021-21063	$^7F_6 - H^o_5$
587.46	M	17017.5	587.42	812-17831	$^7F_2 - {}^7F^o_3$
587.69	M	17010.9	587.59	1490-18503	$^7F_3 - {}^5G^o_4$
589.69	M	16953.2	590.00	812-17770	$^7F_2 - (\ )_1$
			589.52	13458-30416	$^9D_4 - {}^5H^o_5$
590.53	M	16929.0	590.60	1490-18417	$^7F_3 - (\ )_2$
593.71	W	16838.4	593.69	1490-18329	$^7F_3 - {}^7I_3{}^o$
599.11	S	16686.6	598.96	0-16691	$^7F_o - {}^7D^o_1$
602.81	S	16584.2	602.74	1490-18076	$^7F_3 - {}^7H^o_2$
			602.71	3125-19712	$^7F_5 - {}^5F^o_6$

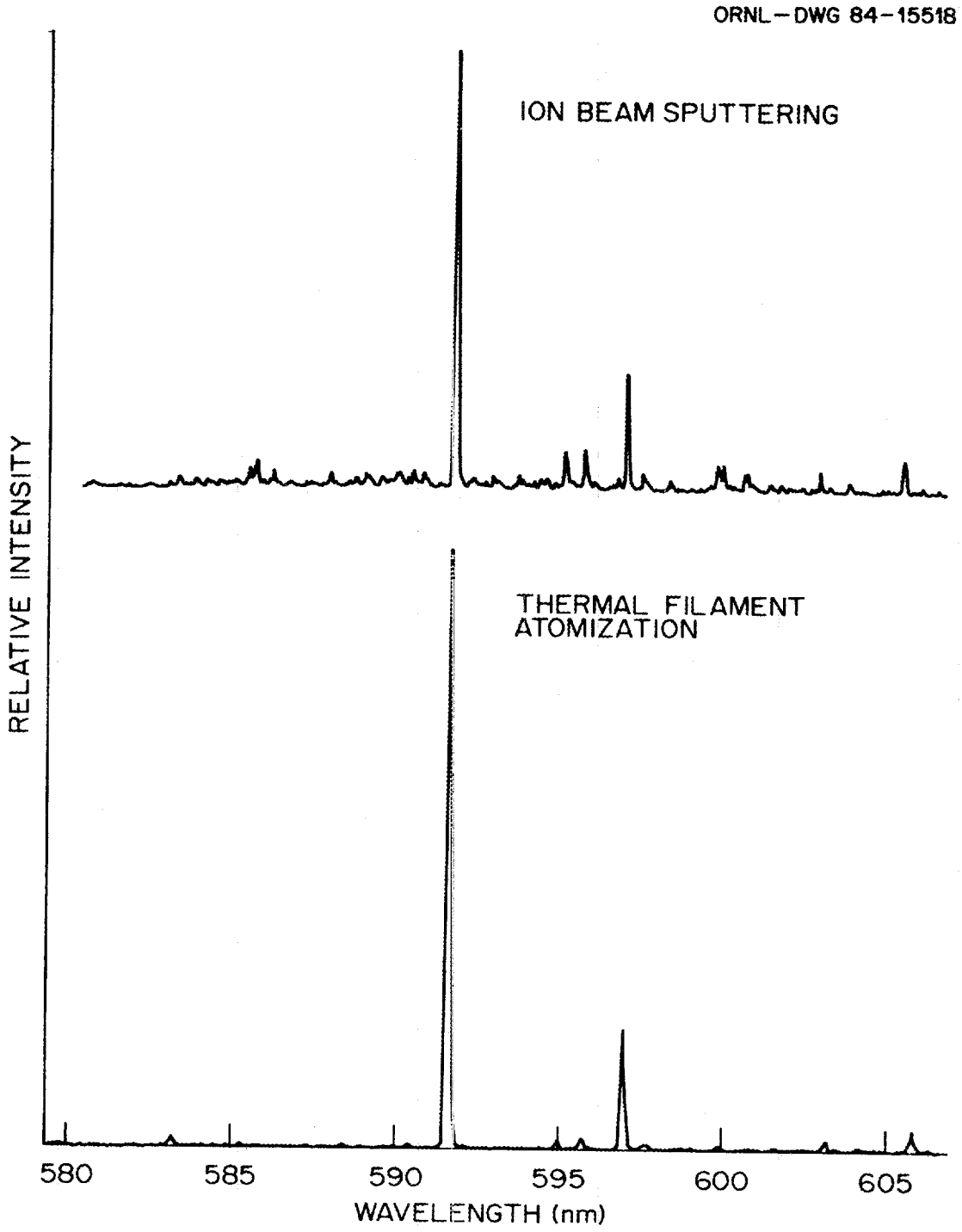

Fig. 7. Optical ionization spectra of ^{238}U atoms produced by ion beam sputtering (top) and thermal filament atomization (bottom)

at 591.54 nm and 596.92 nm are believed to arise from the $^5L^o_6$ ground state and the $^5K^o_5$ (620 cm^{-1}) state, respectively. Again, a three-photon resonant process is invoked using single-color excitation (within the bandwidth of the laser, 3 cm^{-1}). The ratios of the two strongest lines in each case are not significantly different, thus the "temperature" of the sputtered atoms can be compared to that of thermally produced atoms at 1800°C.

3.4 Mass Spectra

It was of interest to know what other ionic species are produced by the laser beam. Therefore, mass spectra were scanned over the mass range 0-300 amu near the resonant wavelengths for U and Sm. Figure 8 shows the results for Sm over a smaller mass region since no other peaks were found outside of this range. At the resonant wavelength of 602.72 nm, the Sm^+ peaks are observed in the expected isotopic abundances between masses 144 and 154. At higher mass, the SmO^+ peaks appear with almost equal intensity in spite of the fact that Ar^+ was the bombarding species. In fact, the SmO^+ peaks occur at all wavelengths produced by the dye laser, indicating a non-resonant ionization process. As an example, the top spectrum in Figure 8 shows the effect of detuning the laser 0.2 nm, resulting in the disappearance of the Sm^+ signal with no change in the SmO^+ intensity.

Figure 9 shows similar results for U at 591.54 and 591.30 nm. The U^+ signal is sharply tunable, while that of UO^+ and UO_2^+ is not. These results suggest that residual oxygen is interacting with the sample to produce metal oxide species which are sputtered and ionized by the laser in a non-resonant process. The SIMS spectra of these metals under Ar^+ bombardment also show strong MO^+ and MO_2^+ peaks. The observed MO^+ formed by laser ionization may result from one or more of the following processes:

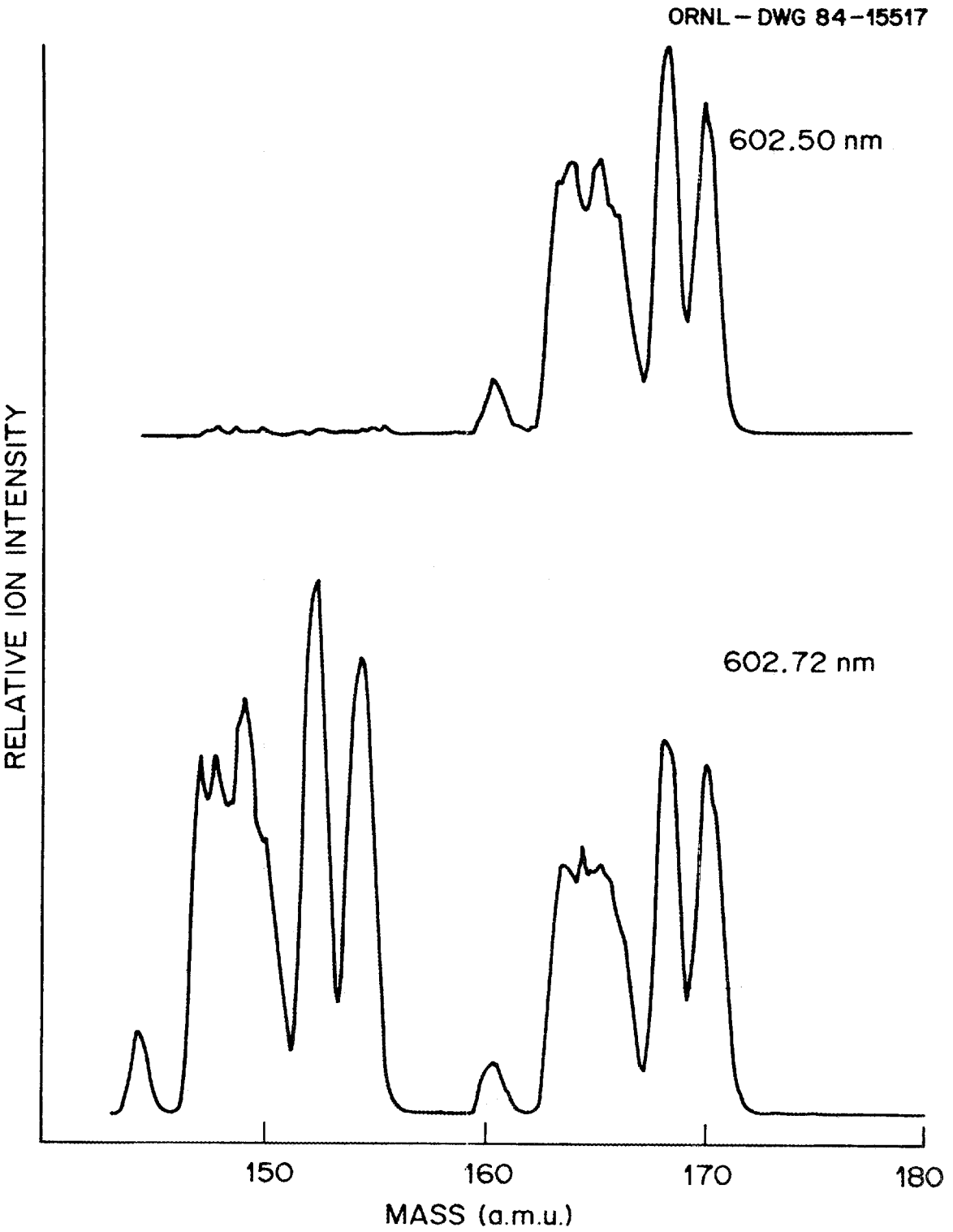

Fig. 8. Mass spectra of Sm produced by laser ionization at 602.50 nm (top) and 602.72 nm (bottom)

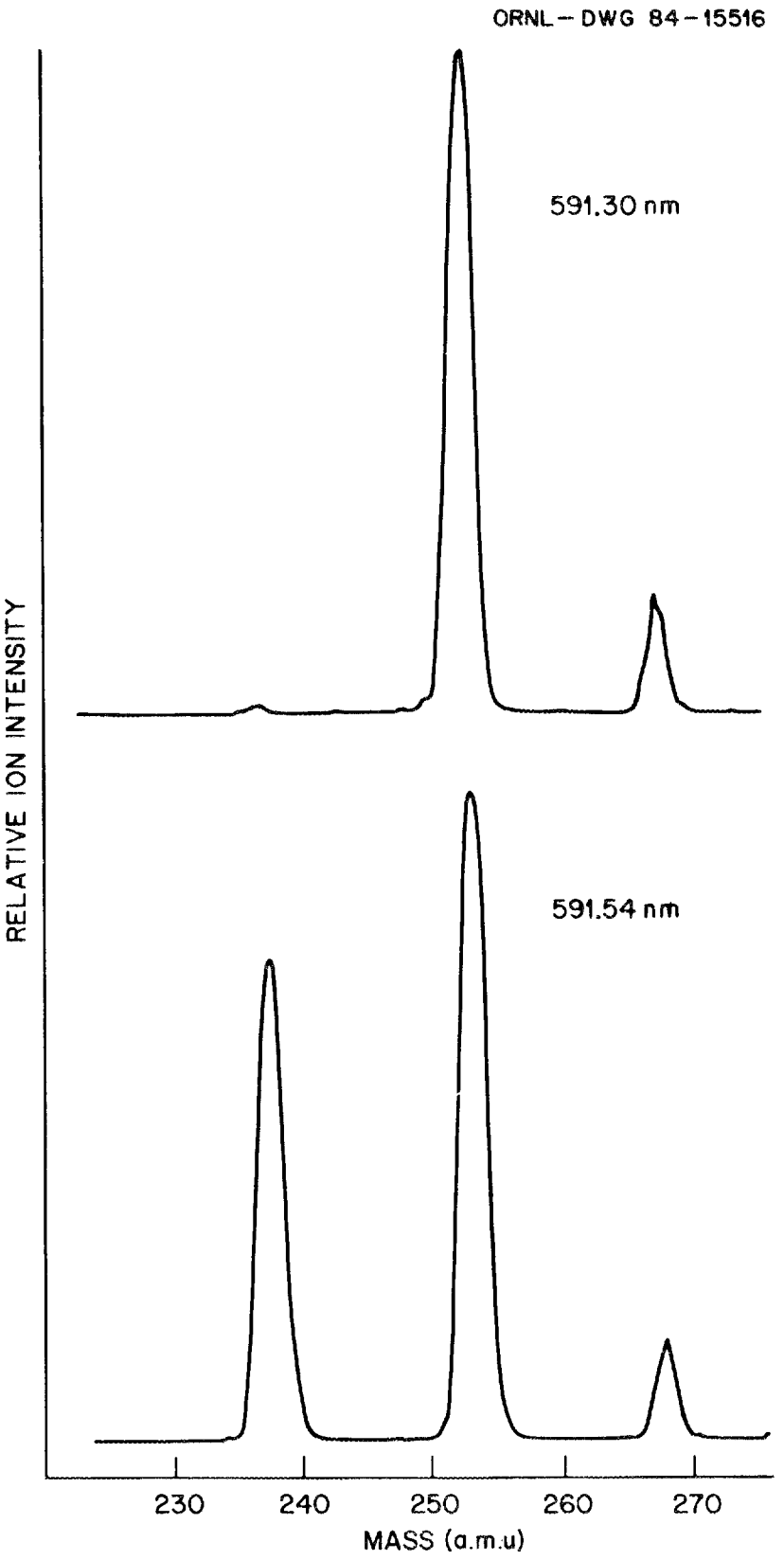

Fig. 9. Mass spectra of U produced by laser ionization at 591.30 nm (top) and 591.54 nm (bottom)

$$MO \xrightarrow{(h\nu)} MO^{+} + e^{-} \quad \text{ionization} \tag{2}$$

$$MO_2 \xrightarrow{(h\nu)} MO^{+} + O^{-} \quad \text{dissociative ionization} \tag{3}$$

$$MO_2 \xrightarrow{(h\nu)} MO^{+} + O + e^{-} \tag{4}$$

This phenomenon will be the subject of further study.

3.5 Future Studies

Future work will involve refinements of the ion optical system to obtain higher extraction and transmission efficiency of the laser generated ions. The use of pulsed ion beam sputtering is being pursued in order to maximize the efficiency of atom production.[18] In addition, a more powerful laser system is being acquired to produce saturated resonance ionization over a larger volume. Investigations of different sample types will involve use of resin beads and small particles of Sm or U oxides, to test the capability of the technique for measuring real-life samples.

References

1. Donohue, D. L.; Young, J. P.; Smith, D. H. Int. J. Mass Spectrom. Ion Phys. 1982, 43, 293-307.

2. Young, J. P.; Donohue, D. L. Anal. Chem. 1983, 55, 88-91.

3. Donohue, D. L.; Young, J. P. Anal. Chem. 1983, 55, 378-379.

4. Donohue, D. L.; Smith, D. H.; Young, J. P.; McKown, H. S.; Pritchard, C. A. Anal. Chem. 1984, 56, 379-381.

5. Young, J. P.; Donohue, D. L.; Smith, D H. Int. J. Mass Spectrom. Ion Processes 1984, 56, 307-319.

6. Miller, C. M.; Cross, J. B.; Nogar, N. S. Optics Comm. 1984, 40, 271-276.

7. Miller, C. M.; Nogar, N. S.; Gancarz, A. J.; Shields, W. R. Anal. Chem. 1982, 54, 2378-2379.

8. Miller, C. M.; Nogar, N. S. Anal. Chem. 1983, 55, 481-488.

9. Miller, C. M.; Nogar, N. S. Anal. Chem. 1983, 55, 1606-1608.

10. Downey, S. W.; Nogar, N. S.; Miller, C. M. Anal. Chem. 1984, 56, 827-828.

11. Fassett, J. D.; Travis, J. R.; Moore, L. J.; Lytle, F. E. Anal. Chem. 1983, 55, 765-770.

12. Fassett, J. D.; Moore, L. J.; Travis, J. L.; Lytle, F. E. Int. J. Mass Spectrom. Ion Processes 1983, 54, 201-206.

13. Fassett, J. D.; Moore, L. J.; Shideler, R. W.; Travis, J. L. Anal. Chem. 1984, 56, 203-206.

14. Savickas, P. J.; Hess, K. R.; Marcus, R. K.; Harrison, W. W. Anal. Chem. 1984, 56, 817-819.

15. Williams, M. W.; Beekman, D. W.; Swan, J. B.; Arakawa, E. T. Anal. Chem. 1984, 56, 1348-1350.

16. Winograd, N.; Baxter, J. P.; Kimock, F. M. Chem. Phys. Lett. 1982, 88, 581-584.

17. Kimock, F. M.; Baxter, J. P.; Winograd, N. Surf. Sci. 1983, 124, L41.

18. Kimock, F. M.; Baxter, J. P.; Pappas, D. L.; Kobrin, P. H.; Winograd, N. Anal. Chem. 1984, 56, 2782-2791.

19. Liebl, H. J. Appl. Phys. 1967, 38, 5277-5283.

20. McGilvery, D. C., Ph.D. Dissertation, LaTrobe University, 1978.

21. Martin, W. C.; Zalubas, R.; Hagan, L., NSRDS-NBS60, National Bureau of Standards, April 1978.

22. Donohue, D. L.; Young, J. P.; Smith, D. H. Appl. Spectros., 1985, 39, 93-97.

Internal Distribution

1. J. A. Carter
2. W. H. Christie
3. D. L. Donohue
4. D. E. Goeringer
5. H. S. McKown
6. R. L. Walker
7. W. D. Shults
8. A. Zucker
9. Central Research Library
10. Document Reference Section
11-12. Laboratory Records Department
13. Laboratory Records Department-RC
14. ORNL Patent Office

External Distribution

DOE, ISA, Forrestal Building, Washington, DC 20585

15. G. F. Dickerson
16. W. A. Emel
17. R. W. Ewing
18. M. A. Koontz
19. R. I. Rubinstein
20. J. L. Torres, Jr.
21. Office of Assistant Manager, Energy Research and Development, DOE, Oak Ridge, TN 37830
22-48. Technical Information Center